JGR Biogeosciences

RESEARCH ARTICLE
10.1029/2018JG004712

Special Section:
Biogeochemistry of Natural Organic Matter

Increasing Organic Carbon Biolability With Depth in Yedoma Permafrost: Ramifications for Future Climate Change

J.K. Heslop[1,2], M. Winkel[1,3], K.M. Walter Anthony[1], R.G.M. Spencer[4], D.C. Podgorski[5], P. Zito[5], A. Kholodov[6], M. Zhang[7], and S. Liebner[3,8]

[1]Water and Environmental Research Center, University of Alaska Fairbanks, Fairbanks, AK, USA, [2]Department of Geography and Planning, Queen's University, Kingston, Ontario, Canada, [3]GFZ German Research Centre for Geosciences, Section 3.7 Geomicrobiology, Helmholtz Centre Potsdam, Postdam, Germany, [4]National High Magnetic Field Laboratory Geochemistry Group and Department of Earth, Ocean, and Atmospheric Science, Florida State University, Tallahassee, FL, USA, [5]Pontchartrain Institute for Environmental Sciences, Department of Chemistry, University of New Orleans, New Orleans, LA, USA, [6]Geophysical Institute, University of Alaska Fairbanks, Fairbanks, AK, USA, [7]School of Natural Resources and Extension, University of Alaska Fairbanks, Fairbanks, AK, USA, [8]University of Potsdam, Institute of Biochemistry and Biology, Potsdam, Germany

Key Points:
- Organic matter quality and greenhouse gas production potentials increase with depth in yedoma permafrost
- CO_2:CH_4 production potentials decrease with depth in yedoma permafrost soils
- Water-extractable organic matter composition depth trends suggest long-term processing under reduced conditions

Supporting Information:
- Supporting Information S1
- Table S1

Correspondence to:
J. K. Heslop,
joannekheslop@gmail.com

Citation:
Heslop, J. K., Winkel, M., Walter Anthony, K. M., Spencer, R. G. M., Podgorski, D. C., Zito, P., et al. (2019). Increasing organic carbon biolability with depth in yedoma permafrost: Ramifications for future climate change. *Journal of Geophysical Research: Biogeosciences*, *124*, 2021–2038. https://doi.org/10.1029/2018JG004712

Received 20 AUG 2018
Accepted 5 JUN 2019
Accepted article online 22 JUN 2019
Published online 12 JUL 2019

Abstract Permafrost thaw subjects previously frozen organic carbon (OC) to microbial decomposition, generating the greenhouse gases (GHG) carbon dioxide (CO_2) and methane (CH_4) and fueling a positive climate feedback. Over one quarter of permafrost OC is stored in deep, ice-rich Pleistocene-aged yedoma permafrost deposits. We used a combination of anaerobic incubations, microbial sequencing, and ultrahigh-resolution mass spectrometry to show yedoma OC biolability increases with depth along a 12-m yedoma profile. In incubations at 3 °C and 13 °C, GHG production per unit OC at 12- versus 1.3-m depth was 4.6 and 20.5 times greater, respectively. Bacterial diversity decreased with depth and we detected methanogens at all our sampled depths, suggesting that in situ microbial communities are equipped to metabolize thawed OC into CH_4. We concurrently observed an increase in the relative abundance of reduced, saturated OC compounds, which corresponded to high proportions of C mineralization and positively correlated with anaerobic GHG production potentials and higher proportions of OC being mineralized as CH_4. Taking into account the higher global warming potential (GWP) of CH_4 compared to CO_2, thawed yedoma sediments in our study had 2 times higher GWP at 12- versus 9.0-m depth at 3 °C and 15 times higher GWP at 13 °C. Considering that yedoma is vulnerable to processes that thaw deep OC, our findings imply that it is important to account for this increasing GHG production and GWP with depth to better understand the disproportionate impact of yedoma on the magnitude of the permafrost carbon feedback.

Plain Language Summary Despite occupying only 7% of global permafrost area, yedoma permafrost contains over a quarter (~398 Gt) of the estimated global permafrost organic carbon (OC) pool. It has been suggested that microbial decomposition of thawed, reactivated OC from yedoma permafrost and subsequent greenhouse gas production may be a "tipping point" for future climate warming. Our research shows that greenhouse gas production potentials increase with depth in yedoma permafrost and, importantly, that following thaw OC from deeper yedoma is more prone to being microbially processed into methane, a potent greenhouse gas with 34 times more global warming potential than carbon dioxide on a century time scale. Considering that yedoma permafrost is particularly vulnerable to processes that deeply thaw permafrost OC, it is crucial to account for this increasing greenhouse gas production and global warming potential per unit OC with depth to better understand how thawing yedoma permafrost will impact global carbon cycling and future climate warming.

1. Introduction

Permafrost, which covers a quarter of the Northern Hemisphere, is considered a vulnerable soil organic carbon (OC) pool (Schuur et al., 2015). As the global climate warms, temperatures in northern high latitudes are increasing at amplified rates, which is projected to continue into the coming century (Myhre et al., 2013). With increasing temperatures, subsequent warming and thawing of permafrost soils removes a major

barrier to OC mineralization, leading to the mobilization and microbial degradation of previously frozen permafrost OC (Schuur et al., 2015). The greenhouse gases (GHG) carbon dioxide (CO_2) and methane (CH_4), produced from thawed permafrost OC, are expected to fuel a positive climate feedback referred to as the permafrost carbon feedback (PCF; Schuur et al., 2015). Natural GHG emissions from wetlands and the PCF could reduce permissible anthropogenic fossil fuel CO_2 emission budgets by up to 15% if temperatures are to stabilize at 1.5 or 2.0 °C above preindustrial levels by 2100 (Comyn-Platt et al., 2018). Further, the PCF was recently shown to be over 2 times larger during the twenty-first century than previously predicted, if abrupt thaw via thermokarst (thaw) lake formation is taken into account, a process that yields high emissions of the more potent greenhouse gas CH_4 (Walter Anthony et al., 2018).

It has been suggested that reactivated OC from thawed yedoma permafrost may be a "tipping point" for future climate warming (Lenton, 2012). Yedoma permafrost formed due to syngenetic sediment, peat, and ice accumulation in unglaciated regions during the Last Ice Age (Schirrmeister et al., 2011; Strauss et al., 2017) and contains high ice and OC contents compared to other mineral-type permafrost soils (Strauss et al., 2017; Zimov et al., 2006). Despite covering only 7% of global permafrost area, yedoma soils contain a substantial portion (~398 Gt; equivalent to approximately 25% of global frozen permafrost OC) of thaw-susceptible OC (Strauss et al., 2017). Permafrost OC biolability is known to be controlled by both the OC molecular composition and redox state (Herndon et al., 2015; Schädel et al., 2014) as well as the microbial community structure and its response to permafrost thaw (Graham et al., 2012). Yedoma OC has been previously shown to be highly biolabile upon thaw (Dutta et al., 2006; Knoblauch et al., 2013, 2018; Vonk et al., 2013). Studies of dissolved organic carbon (DOC) and total OC mobilized from yedoma permafrost have also found high proportions (17–62%; Mann et al., 2014; Spencer et al., 2015; Vonk et al., 2013; Walter Anthony et al., 2014) of yedoma OC are bioavailable upon thaw. In comparison, nonyedoma-type permafrost has been estimated to have 5–30% of its OC to be bioavailable upon thaw (Schädel et al., 2014). The higher proportions of bioavailable OC in yedoma-type permafrost are postulated to be due to yedoma OC having low decomposition rates during Pleistocene deposition, the OC not having undergone Holocene decomposition, and the ancient organic matter (OM) containing higher proportions of biolabile, energy-rich, and low molecular weight moieties (Drake et al., 2015; Ewing et al., 2015; Spencer et al., 2015; Strauss et al., 2017).

The syngenetic formation of yedoma sediment profiles, coupled with the presence of unfrozen water, creates conditions where viable microbial communities can survive (Mackelprang et al., 2017; Rivkina et al., 2000). Prior characterization of microbial communities in deep yedoma permafrost suggests active microbial metabolic processes in permafrost soils, but low microbial biomass and diversity (Mackelprang et al., 2017; Wagner et al., 2007). Following thaw, suitable conditions could allow for the activation of microbial communities, including methanogens, and subsequent GHG production (Knoblauch et al., 2018; Mackelprang et al., 2011; Wei et al., 2018). However, microbial communities in deep permafrost remain a relatively unknown component, and we cannot currently predict how microbes will use permafrost OC following thaw (Graham et al., 2012; Malard & Pearce, 2018).

With climatic warming or when subjected to ground-surface disturbance, yedoma is prone to thermokarst activity including deep thermokarst lake formation, which can strongly alter the local thermal balance, trigger rapid permafrost thaw and talik (thaw bulb) formation, and mobilize OC from deep yedoma permafrost for mineralization under anaerobic conditions (Heslop et al., 2015; Kessler et al., 2012; Schneider von Deimling et al., 2015). Once formed, thermokarst lakes and their taliks provide a direct conduit for CO_2 and CH_4 produced within deep, old yedoma OC to be emitted directly to the atmosphere (Walter Anthony et al., 2016). Old OC from deep yedoma can also be thawed and mineralized following thermoerosion along coasts (Vonk et al., 2017) and rivers (Kanevskiy et al., 2016). With twenty-first-century climate warming, rapid, deep thaw processes such as thermokarst lake formation are anticipated to increase old (^{14}C-depleted) permafrost soil OC fluxes 125% to 190% compared to gradual permafrost thaw via active layer thickening (Walter Anthony et al., 2018). Other nonlake mechanisms of abrupt thaw, such as thermoerosional gullies, thaw slumps, and peat-plateau collapse scars, will further increase permafrost carbon emissions (Olefeldt et al., 2016). Therefore, it is critical to understand how OC biodegradability changes with depth to estimate the strength of the PCF, especially for permafrost such as yedoma that is prone to deep thaw.

Here we sought to determine how yedoma OC biodegradability, and by extension potentials for CO_2 and CH_4 production, changes with depth in anaerobic conditions consistent with a thermokarst-lake

environment. We examined the molecular composition of water-extractable organic matter (WEOM) and microbial community composition from a yedoma permafrost profile in central Alaska in conjunction with anaerobic carbon (C) mineralization potentials of the thawed OC under two temperature scenarios (3 and 13 °C). We anticipated that specific WEOM compound classes and/or microbial taxa would emerge as indicators of anaerobic C mineralization potentials from the thawed permafrost sediments. To our knowledge, this is the first study to use a combination of incubation data, molecular composition of WEOM, and microbial community composition to specifically address how OC biodegradability and GHG emissions change with depth, and thus has important ramifications for future predictions on the strength of the PCF.

2. Methods

2.1. Study Site and Sampling

The Vault Creek (VC) permafrost tunnel (65°01′46.3″N, 147°42′22.4″W), located in the Chatanika River Valley 20 km north of Fairbanks, AK, USA, was excavated in 1990 by a local private gold miner. The region experiences a continental climate with a mean annual air temperature of −2.39 °C and 274.6mm mean annual precipitation (Fairbanks International Airport 1981–2010, National Climate Data Center). Permafrost in this region is discontinuous (Jorgenson et al., 2008) and relatively warm (mean annual temperature −0.7 °C at the tunnel site; Schirrmeister et al., 2016). An adjacent first-generation thermokarst lake (Vault Lake, informal name), described in detail by Heslop et al. (2015), indicates that local thermokarst activity is actively thawing permafrost both laterally and vertically within the landscape. Sediment characteristics and paleoenvironmental records from the VC permafrost tunnel have been previously studied by Meyer et al. (2008) and Schirrmeister et al. (2016).

In this study, we collected and examined soil samples from four horizons in the VC permafrost tunnel that can potentially be thawed due to thermokarst activity and the formation of a thermokarst-lake talik. The entrance of the VC permafrost tunnel is secured by a steel tube, making the top 4 m of the vertical soil profile inaccessible from the tunnel. Therefore, we collected samples from the modern active layer (AL; 0.7-m depth) and the transitional permafrost (TL; 1.3-m depth) using a SPIRE drill. The AL sample represents soils in the modern active layer that currently experience seasonal freezing and thawing; the TL sample represents yedoma soils which thawed ~5,000–7,000 years ago during the Holocene thermal optimum, subsequently refroze, and remained frozen until the present (Kanevskiy et al., 2011). At the VC permafrost tunnel site, the transition from the AL to the TL layer was identified using cryostratigraphy. We identified a 3–4mm thick horizontal ice lens at 94-cm depth accompanied by an abrupt change from microlenticular ground ice with ice veins up to 3 mm thick to porous ground ice. Two deeper yedoma soil samples (Y-9m and Y-12m, 9- and 12-m depth, respectively) were collected from the walls of the VC permafrost tunnel using an axe and hammer. Samples for bulk density were collected with a hole saw. These samples are representative of deep yedoma permafrost that formed during the Pleistocene and remained frozen until present, as evidenced by intact Pleistocene ice wedges surrounding the ice-rich frozen soil samples. All soil samples were collected during February 2016 and were kept frozen at −10 °C until further analyses.

2.2. Anaerobic Incubation

Soil samples collected from each of the four depths were anaerobically incubated at two temperatures (3 and 13 °C) selected to be representative of temperatures observed in the talik beneath the adjacent thermokarst lake (Heslop et al., 2015). We prepared sediment slurries using homogenized sediment and O_2-free, sterilized DI water (mean ± SD 392 ± 63 g dry weight sediment/L slurry) under anaerobic conditions in a glove bag filled with ultrahigh-purity N_2 gas. Three subsamples of the slurry were reserved for geochemical, microbial, and WEOM analyses; 60 mL of the slurry was transferred to 100-mL glass serum bottles, which were then capped with butyl rubber stoppers and crimped to seal. Anaerobic conditions in the incubation vials were verified by sampling a subset of incubation vials using an airtight syringe and measuring headspace O_2 concentrations using gas chromatography (Shimadzu GC-2014). Headspace CO_2 and CH_4 concentrations in each incubation vial, collected using an airtight syringe, were measured in monthly time steps for a 154-day incubation period using gas chromatography (Shimadzu GC-2014; Figures S1 and S2). At the end of the 154-day incubation period, all incubation vials were destructively sampled and the sediment slurries were reserved for WEOM analyses, described below.

Anaerobic C mineralization potentials were calculated from measured headspace CO_2 and CH_4 concentrations using Henry's law and normalized by the initial mass of soil OC (SOC) in each bottle (μg C g SOC^{-1} d^{-1}). Henry's law constants for CO_2 ($k°_H$ = 0.034 mol/kg*bar) and CH_4 ($k°_H$ = 0.0013 mol/kg*bar) were obtained from the National Institute of Standards and Technology Chemistry WebBook. Net C mineralization potential in each incubation vial was calculated as the sum of C-CO_2 and C-CH_4 production potentials. The global warming potential (GWP) of each incubation vial was calculated by converting C-CH_4 production into CO_2 carbon equivalents (CE) by multiplying C-CH_4 production by a GWP of 34 over 100 years (Schädel et al., 2016), then summing the value with C-CO_2 production (mg C-CO_2 CE g SOC^{-1}). All C mineralization potential values are presented as the mean ± standard deviation (SD) of the triplicate vials at each sample depth and incubation temperature.

Due to the potential presence of alternative electron acceptors in the sediment slurry and the need for stable CH_4-producing communities to establish in incubation vials, steady state CH_4 production in anaerobic incubations can experience lag times ranging from weeks to years (Knoblauch et al., 2013, 2018). To account for potential lag phases in steady state CH_4 production in our incubations, we compare net GHG production potentials measured at the end of our 154-day incubation as opposed to GHG production potential rates. Using C mineralization potentials measured at the end of the anaerobic incubation, Q_{10} values for each depth were calculated as the ratio of mean net C mineralization potentials (C-CO_2 + C-CH_4) between the 3 and 13 °C incubation temperatures.

2.3. Soil Geochemistry and Water-Extractable Organic Matter Characterization

One subsample of the initial slurry (collected prior to incubation as described above) was oven-dried (105 °C for 48 hr), homogenized using a mortar and pestle, and analyzed for total C (C_{tot}), total nitrogen (N_{tot}), organic C (C_{org}), C_{org}:N_{tot} ratios, and stable isotopic values ($\delta^{13}C_{org}$ and $\delta^{15}N_{tot}$) using a Finnigan DeltaPlus XP elemental analyzer (Thermo Scientific) coupled to a Costech ECS4010 elemental analyzer (Costech Scientific) at the University of Alaska Stable Isotope Facility, Fairbanks, AK, USA. Inorganic C content ($C_{inorganic}$) was calculated as the difference between C_{tot} and C_{org} content. A second slurry subsample, also collected prior to incubation, was filtered through a precombusted (450 °C for 4 hr) glass microfiber filter (0.7 μm, Whatman GF/F) to remove particulate organic matter. A subsample of the filtered slurry was analyzed for ammonium (N-NH_4^+), nitrate and nitrite (N-NO_2^- + N-NO_3^-), total iron (Fe), and manganese (Mn) contents using an elemental analyzer at the University of Alaska, Fairbanks. The remaining filtered slurry was kept frozen at −10 °C until further WEOM analyses described below. An additional set of filtered slurry subsamples were collected at the end of the 154-day anaerobic incubation, filtered through a precombusted (450 °C for 4 hr) glass microfiber filter (0.7 μm, Whatman GF/F) to remove particulate organic matter, and kept frozen at −10 °C until further analyses.

The filtered slurry subsamples from both the beginning and the end of the 154-day anaerobic incubation were analyzed for dissolved organic carbon (DOC) content using a Shimadzu TOC-L CPH at Florida State University. DOC concentration (mg C/L) was divided by the mass of dry sediment per unit volume in the corresponding slurry (g dw/L) to determine soil water-extractable organic carbon (WEOC) content (mg C/g dw). Samples were prepared for Fourier transform ion cyclotron resonance mass spectrometry (FT-ICR MS) analysis using the solid-phase dissolved organic matter (DOM) extraction method (Dittmar et al., 2008). Filtered slurry sample volume used for solid phase extraction was adjusted based on the DOC concentration of each sample to obtain a 50 μg C/mL methanol eluate. Extracts were analyzed on a custom-built 9.4-T FT-ICR mass spectrometer with a 22-cm-diameter horizontal bore at the National High Magnetic Field Laboratory, Tallahassee, FL, USA (Kaiser et al., 2011). Negative ions were generated using direct infusion electrospray ionization at a rate of 500 nL/min; 100 time domain acquisitions were co-added for each mass spectrum. Molecular formulae were assigned to each spectra using in-house software (EnviroOrg©™ Software E 2.0; Corilo, 2015) at the National High Magnetic Field Laboratory based on published rules (Koch et al., 2007; Stubbins et al., 2010). Molecular formulae with elemental combinations of $C_{1\text{-}45}H_{1\text{-}92}N_{0\text{-}4}O_{1\text{-}25}S_{0\text{-}2}$ were considered for assignment. Each formula was classified based on their elemental stoichiometries (Santi-Temkiv et al., 2013) and a modified aromaticity index (AI) calculated for each formula (Koch & Dittmar, 2006). Based on the elemental stoichiometries and AI of each molecule, for the purposes of this study we classified compounds into six compound classes (O'Donnell et al., 2016): condensed aromatics (AI ≥ 0.67), polyphenolic (0.5 < AI < 0.67), unsaturated low oxygen (AI < 0.5, H/C

< 1.5, O/C < 0.5), unsaturated high oxygen (AI < 0.5, H/C < 1.5, O/C > 0.5), aliphatics (1.5 < H/C < 2.0, O/C < 0.9, N = 0), and peptide-like (1.5 < H/C < 2.0, O/C < 0.9, N > 0). WEOM compound class data are presented as relative abundance (%) of identified formulae. In this study we interpret compound classes based on relative abundance, which reflects the signal magnitude of compounds that are detected during FT-ICR MS and the number of molecular formulae assigned to that compound class.

Changes in the relative abundance of WEOM compounds and compound classes were calculated at both incubation temperatures using equation (1):

$$\%\text{Change} = \frac{A_{\text{final}} - A_{\text{initial}}}{A_{\text{initial}}} \quad (1)$$

where A_{initial} is the initial relative abundance (%) of compound or compound class A in the vial and A_{final} is the relative abundance (%) of compound or compound class A in the vial at the end of the 154-day incubation. Positive values indicate the relative abundance increased during the incubation, while negative values indicate the relative abundance decreased during the incubation.

2.4. Microbial Analyses

A third subset of slurry subsamples, collected at the beginning of the incubation period, were immediately frozen at −80 °C and kept frozen until further analyses. Genomic DNA of 4.7–13-g sediment was extracted using the protocol of Zhou et al. (1996). DNA concentrations were quantified with a Nanophotometer® P360 (Implen GmbH) and Qubit® 2.0 Flurometer (Thermo Fisher Scientific).

The 16S rRNA gene for bacteria was amplified with the primer combination S-D-Bact-0341-a-S-17 and S-D-Bact-0785-a-A-21 (Herlemann et al., 2011). The 16S rRNA gene for archaea was amplified in a nested approach with the primer combination S-D-Arch-0020-a-S-19 and S-D-Arch-0958-a-A-19 in the first polymerase chain reaction (PCR) for 40 cycles and S-D-Arch-0349-a-S-17 and S-D-Arch-0786-a-A-20 in the second PCR for 35 cycles, respectively. The primers were labeled with unique combinations of barcodes. The PCR mix contained 1× PCR buffer (Tris•Cl, KCl, $(NH_4)2SO_4$, 15 mM $MgCl_2$; pH 8.7; QIAGEN), 0.5 μM of each primer (Biomers), 0.2 mM of each deoxynucleoside (Thermo Fisher Scientific), and 0.025 U/μL hot start polymerase (QIAGEN). The thermocycler conditions were 95 °C for 5 min (denaturation), followed by 40 cycles of 95 °C for 1 min (denaturation), 56 °C for 45 s (annealing), and 72 °C for 1 min and 30 s (elongation), and concluding with a final elongation step at 72 °C for 10 min. PCR products were purified with a Hi Yield® Gel/PCR DNA fragment extraction kit (Süd-Laborbedarf). PCR products of three individual runs per sample were combined. PCR products of different samples were pooled in equimolar concentrations and compressed to a final volume 10 μL with a concentration of 200 ng/μL in a vacuum centrifuge Concentrator Plus (Eppendorf). Individual samples were sequenced in duplicates. Illumina sequencing was performed by GATC Biotech AG using 300-bp paired-end mode. Due to different sequencing length, we used 20% PhiX control v3 library for better performance.

The quality of the sequences was checked using the fastqc tool (http://www.bioinformatics.babraham.ac.uk/projects/fastqc/by S. Andrews). Sequence raw reads were demultiplexed and barcodes were removed with the CutAdapt tool (trim-n; e 0.1; only consider exact barcodes for mapping; Martin, 2011). The subsequent steps included merging of reads using overlapping sequence regions PEAR (Q 25; p 0.0001; v 20; Zhang et al., 2014), standardizing the nucleotide sequence orientation, and trimming and filtering of low-quality sequences using Trimmomatic (SE; LEADING Q25; TRAILING Q25; SLIDINGWINDOW 5:25; MINLEN 200; Bolger et al., 2014). After quality filtering, chimera were removed by the ChimeraSlayer tool of the QIIME pipeline. Subsequently, sequences were clustered into operational taxonomic units (OTU) at a nucleotide cutoff level of 97% similarity and singletons were automatically deleted. To reduce noise in the data set, sequences with relative abundances below 0.1% per sample were also removed. All archaeal libraries contained at least >14.300 sequences, while bacterial libraries contained at least >71.400 sequences. OTUs were taxonomically assigned employing the Silva database release 128 (Quast et al., 2012) using the QIIME pipeline (Caporaso et al., 2010). Older taxonomic assignments for archaea and bacteria were manually corrected (e.g., Miscellaneous Crenarchaeal Group (MCG) was renamed to *Bathyarchaeota*) using taxonomies described in Rinke et al. (2013), Castelle et al. (2015), and Adam (2017).

Table 1
Initial Sediment and Slurry Geochemistry for Each Sample Depth

	Sample[a]			
Depth (m)	AL 0.7 m	TL 1.3 m	Y-9m 9 m	Y-12m 12 m
Sediment geochemistry				
C_{tot} (wt %)	0.74	1.79	1.99	3.91
C_{org} (wt %)	0.44	1.58	1.45	2.26
$C_{inorganic}$ (wt %)	0.30	0.22	0.54	1.65
N_{tot} (%)	0.05	0.16	0.19	0.33
C_{org}:N_{tot}	8.2	9.6	7.7	6.8
$\delta^{13}C_{org}$ (‰)	−25.2	−25.6	−25.0	−26.5
$\delta^{15}N$ (‰)	5.5	3.4	4.0	1.8
WEOC (mg C/g dw)	14.0	85.0	597	1454
WEOC:C_{org}	31.8	53.8	412	642
Slurry geochemistry				
DOC (mg/L)	6.78	33.98	227.8	443.5
N-NH_4^+ (mg/L)	0.22	0.72	3.80	36.3
N-NO_2^- + N-NO_3^- (mg/L)	0.00	0.02	0.23	4.19
Total Fe (mg/L)	5.05	1.23	18.75	21.72
Mn (mg/L)	0.04	1.52	1.83	0.95

[a]AL = active layer, TL = transitional permafrost layer, Y-9m = 9-m yedoma permafrost, Y-12m = 12-m yedoma permafrost.

Sequences have been deposited at NCBI under the Bioproject PRJNA432510 with the sequence read archive accession numbers SRR6740235, SRR6740237, SRR6740232, and SRR6740246 for bacterial and SRR6729506, SRR6729504, SRR6729509, and SRR6729533 for archaeal sequences, respectively.

Quantitative PCR was performed using the CFX Connect™ Real-Time PCR Detection System (Bio-Rad Laboratories). Each reaction contained iTaq™ Universal SYBR® Green Supermix (12.5 μL per reaction of 2× concentrate, Bio-Rad Laboratories), PCR primers (0.5 μL containing 20 μM each), sterile water (6.5 μL), and DNA template (5 μL) added to a final volume of 25 μL. Primers mlas and *mcrA*-rev (Steinberg & Regan, 2008) were used to targeting the functional gene *mcrA*. The PCR reactions comprised an initial denaturation (5 min at 95 °C), followed by 40 cycles of 5 s at 95 °C, 30 s at 57 °C specific annealing temperature,10 s at 72 °C, and a plate read step at 80 °C for 3 s. Melt curve analysis from 65 to 95 °C with a 0.5 °C temperature increment per cycle (5 s) was conducted at the end of each run to check for nonspecific amplification of DNA. The qPCR assays were calibrated using known amounts of PCR amplified and cloned gene fragments from corresponding taxa (standards of pure cultures) in the range of 10^6–10^1 copies/μL. Prior to qPCR analysis, DNA templates were diluted 5- to 100-fold and triplicates were analyzed for each sample. The PCR efficiency based on the standard curve was calculated using the Bio-Rad CFX Manager software and was 95%. All cycle data were collected using the single-threshold Cq determination mode. Initial *mcrA* copies were below detection limit (detection threshold 10^2 copies/g) at all four sample depths.

2.5. Statistics

All statistical analyses were conducted using MATLAB R2016a software. We treated each of our triplicate incubation vials as one observation in our statistical analyses, as opposed to defining one observation as mean values calculated from the triplicate vials at each sample depth and incubation temperature. Because not all input parameters were consistent with a normal distribution, correlations were calculated using nonparametric Spearman's rho. Correlations were considered statistically significant when $p \leq 0.10$.

3. Results

3.1. Initial Sediment Geochemistry and WEOM Characterization

In our permafrost profile, initial sediment concentrations of C_{org}, N_{tot}, and WEOC increased with depth (Table 1). Initial slurry concentrations of DOC, N-NH_4^+, N-NO_2^- + N-NO_3^-, and total Fe also increased with depth (Table 1). The initial abundance of condensed aromatic compounds was higher in soils from the AL and TL horizons (13.9 ± 0.6%) than soils from the yedoma permafrost (8.9 ± 1.6%; Figure 1). We also observed higher initial abundance of aliphatics and peptide-like compounds (low O/C, high H/C compounds) in soils from the deep yedoma permafrost (9.7 ± 1.4% and 5.1 ± 4.0% for aliphatics and peptide-like, respectively) compared to soils from the AL and TL horizons (4.5 ± 1.2% and 0.4 ± 0.3%; Figure 1). Results from correlation of initial sediment and slurry geochemical characteristics and WEOM characteristics are presented in Figure S3 in the supporting information.

3.2. Anaerobic C Mineralization Potentials and Changes in WEOM Composition

In the soil samples from the perennially frozen permafrost (TL, Y-9m, Y-12m), both net anaerobic C mineralization (mg C/g SOC) and Q_{10} values increased with depth (Table 2 and Figures S1 and S2). Apart from the Y-12m sample at 3 °C, C-CO_2:C-CH_4 ratios decreased with depth at both incubation temperatures (3 and 13 °C; $p < 0.05$; Table 2). The initial relative abundance of unsaturated low and high oxygen compounds negatively correlated with anaerobic C-CO_2 production and net C mineralization at both incubation temperatures (3 and 13 °C) during our 154-day incubation (Figures 2 and S4 and Table S1). Initial relative abundance of aliphatic compounds positively correlated with C-CH_4 production (13 °C) and net C

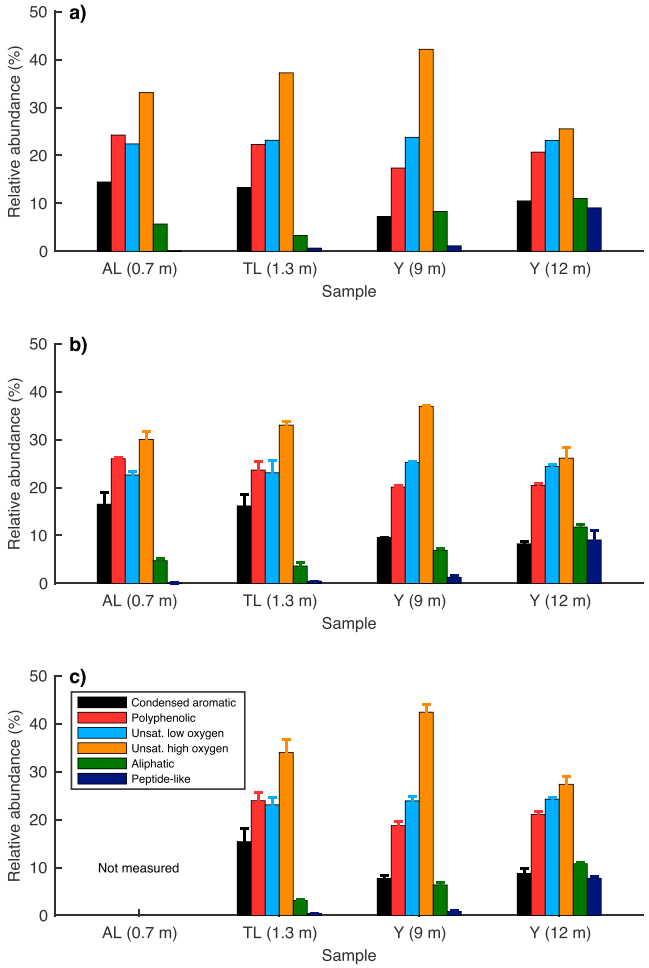

Figure 1. Relative abundance of WEOM compound classes at (a) the beginning and (b, c) end of the 154-day anaerobic incubation at two temperatures: (b) 3 °C and (c) 13 °C. WEOM composition was measured using FT-ICR MS analyses and identified formulae were classified into six compound classes based on their elemental stoichiometries and a modified aromaticity index.

mineralization (3 and 13 °C; Figure S5). C-CH_4 production at the 13 °C incubation temperature also negatively correlated with initial relative abundance of condensed aromatic and polyphenolic compounds and positively correlated with initial relative abundance of peptide-like compounds. Full initial sediment geochemistry and WEOM characterization correlation with anaerobic C mineralization results are presented in Table S1 in the supporting information.

The changes in relative abundance of aliphatic and condensed aromatic compounds (Figures 3a, 3e, 4a, and 4e) for some depths were higher than relative changes of the remaining compound classes. With the exception of the Y-12m sample, relative abundance of aliphatic compounds generally decreased during the 154-day anaerobic incubation at both temperatures (Figures 3e and 4e) while the relative abundance of condensed aromatic compounds increased during anaerobic incubation (Figures 3a and 4a). Full results are presented in Figures S6 and S7 in the supporting information.

3.3. Microbial Community Characterization

Bacterial diversity, quantified using the Inverse Simpson Index, significantly decreased with depth in our profile ($p < 0.05$; Figure 5). We observed lower archaeal diversity in the TL horizon compared to our remaining depths ($p < 0.05$), but no statistically significant trends in archaeal diversity with depth. Methanogens were detected at all four sampled depths using 16S RNA sequencing; however, initial *mcrA* copies, an indicator of methanogen biomass, were below detection limit (detection threshold 10^2 copies/g) at all four sampled depths at the start of the incubation.

4. Discussion

4.1. Organic Matter Characteristics

In the VC permafrost tunnel, we observed higher concentrations of N-NH_4^+, N-NO_2^- + N-NO_3^-, and total Fe in our initial slurries with depth, and increasing proportions of inorganic N being in the reduced NH_4^+ state versus the oxidized NO_2^- and NO_3^- states (Table 1). We interpret these data as evidence of long-term (millennial time scales) anoxia in yedoma permafrost leading to reduced conditions (Ewing et al., 2015). We concurrently observed increases in DOC and WEOC concentrations and WEOC:C_{org} ratios with depth (Table 1). Ewing et al. (2015) also found increasing DOC concentrations with depth in a yedoma core collected from near Livengood, AL, which were attributed to DOC production and mineral dissolution under reducing conditions. These increasing WEOC and WEOC:C_{org} ratios observed with depth suggest that, with increasing depth, greater proportions of SOM are in a form that can be directly utilized by microbes.

A unique aspect of our study is our examination of the molecular composition of WEOM, as opposed to the composition of total soil OM or DOM collected in permafrost-underlain watersheds. While concentrations of WEOM are small compared to the total soil OM pool, WEOM represents the most mobile and biolabile fraction of soil OM (Szymański, 2017) that can be directly utilized by microbes (Wang et al., 2014). To the best of our knowledge only two studies have previously characterized WEOM from deep permafrost (Drake et al., 2015; Ewing et al., 2015). Most studies examining potential biolability of thawed permafrost OC, especially deep yedoma permafrost OC, characterize the total soil OM pool (Knoblauch et al., 2013; Schädel et al., 2014, 2016; Stapel et al., 2016, 2017; Strauss et al., 2015). However, WEOM has previously been shown to be a stronger predictor of microbial activity than soil OM (Haney et al., 2012). Studies of DOM measured in yedoma-dominated watersheds support that the dissolved fraction of the total OM pool is particularly

Table 2
Anaerobic C-CO_2, C-CH_4, Net C, GWP, and C-CO_2:C-CH_4 Ratios for Each Sample Depth

	Sample			
Depth (m)	AL 0.7 m	TL 1.3 m	Y-9m 9 m	Y-12m 12 m
T = 3 °C				
C-CO_2 (mg C/g SOC)	5.94 (0.52)	2.86 (0.02)	3.09 (0.53)	13.4 (2.08)
C-CH_4 (mg C/g SOC)	0.04 (0.06)	0.10 (0.13)	0.24 (0.29)	0.25 (0.31)
Net C (mg C/g SOC)	5.99 (0.56)	2.96 (0.14)	3.33 (0.77)	13.7 (1.89)
GWP (mg C-CO_2 CE[a]/g SOC)	7.45 (2.53)	6.30 (4.35)	11.1 (10.2)	22.1 (9.22)
C-CO_2:C-CH_4	134	28	13	53
T = 13 °C				
C-CO_2 (mg C/g SOC)	10.7 (2.23)	5.25 (0.57)	6.05 (0.52)	17.6 (2.04)
C-CH_4 (mg C/g SOC)	0.16 (0.20)	1.33 (1.61)	7.58 (7.39)	117 (4.33)
Net C (mg C/g SOC)	10.9 (2.43)	6.58 (1.10)	13.6 (7.69)	135 (2.31)
GWP (mg C-CO_2 CE[a]/g SOC)	17.1 (8.91)	50.6 (54.3)	263 (252)	4009 (145)
C-CO_2:C-CH_4	37	3.9	0.8	0.2
Q_{10} (net C, 3 °C to 13 °C)	1.8	2.2	4.1	9.9

Values are mean (SD) cumulative C mineralization among triplicate vials during the 154-day incubation.
[a]CE = carbon equivalent.

biolabile (Mann et al., 2014; Spencer et al., 2015; Vonk et al., 2013) and, though small, is relevant for estimating GHG production potentials from thawing permafrost. While the DOM measured in these studies partially originates from thawed permafrost OM, it is also influenced by additional DOM sources in the watershed and in situ processing, making it difficult to identify and trace permafrost-derived DOM in these systems (Drake et al., 2018).

By experimentally extracting WEOM in our study, we were able to specifically determine the composition and biolability of permafrost-derived DOM. The WEOM in our yedoma permafrost profile contained increasing abundances of reduced (low O/C), saturated (high H/C) compounds (aliphatics and peptide-like compounds), and decreasing abundance of condensed aromatic compounds with depth (Figure 1). Relative abundance of aliphatic and peptide-like compounds in the modern active layer is likely influenced by depletion via microbial processing during seasonal thawed periods. Combined aliphatic and peptide-like relative abundances of 9.45 and 20.1% in the yedoma samples are high for mineral soils, and are comparable with aliphatic and peptide-like relative abundance observed in more organic soil horizons (O'Donnell et al., 2016). We suggest that the trend of increasing aliphatic and peptide-like compounds relative abundance with increasing depth in the permafrost samples provides further evidence of OM compounds being reduced and preserved in a highly biolabile state over millennial time scales in the energy-limited yedoma permafrost environment.

Evidence of reducing conditions influencing permafrost OM composition over millennial time scales has also been observed in yedoma permafrost cores from northeast Siberia (Stapel et al., 2016, 2017) and at a different location in interior Alaska (Ewing et al., 2015). In a yedoma permafrost core collected from northeast Siberia, sediments deposited during climatic conditions of the late Pleistocene glacial periods had increased aliphatic and acetate concentrations compared to sediments from the same core deposited during interglacial periods and the Holocene (Stapel et al., 2017). The sediments deposited during glacial periods also had higher abundances of biomarkers for past microbial communities, suggesting that the increased aliphatic and acetate concentrations may have also been influenced by climatic conditions and microbial processing during deposition (Stapel et al., 2016, 2017). At the VC permafrost tunnel, paleobotanical proxy data from our sampled depths suggest that climatic conditions at the time of sediment deposition were relatively warm, wet, and similar to Holocene conditions (Schirrmeister et al., 2016). Yedoma cores collected from similar depths to our study from near Livengood, AL show increasing acetate concentrations with sediment age (Ewing et al., 2015), suggesting that the variation in WEOM composition we observed at the VC permafrost tunnel may be due to processing following permafrost formation. Each of these studies (this study; Ewing et al., 2015; Stapel et al., 2016, 2017) point to the importance of OM processing, both during

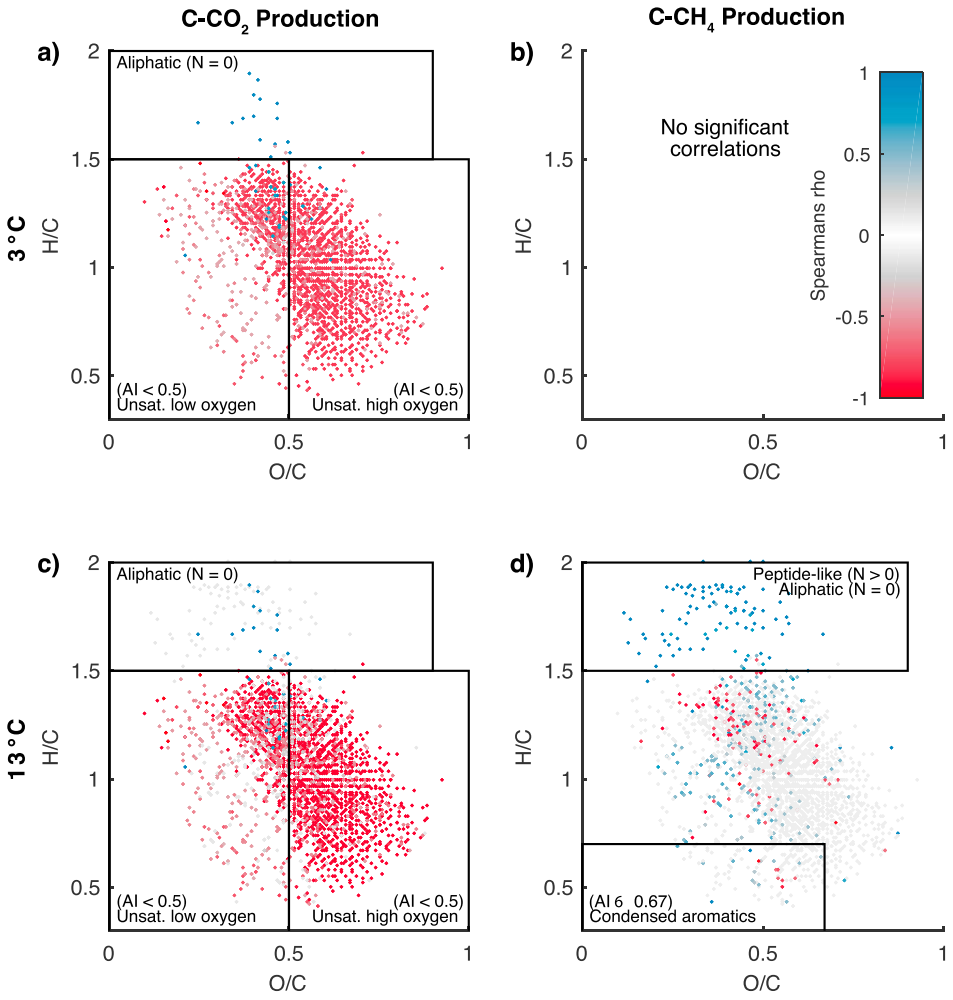

Figure 2. Spearman's rho correlation coefficients of initial identified WEOM compounds versus anaerobic C mineralization potentials at all sampled depths during the 154-day incubation at two temperatures: (a and b) 3 °C and (c and d) 13 °C. Correlations are shown with C-CO_2 production (a and c) and C-CH_4 production (b and d). Because not all input parameters were consistent with a normal distribution, correlation was calculated using nonparametric Spearman's rho. Only significant ($p > 0.10$) correlations are shown; boxed regions represent compound classes which significantly ($p > 0.10$) correlated with C mineralization (Table S1). We did not observe any statistically significant correlation ($p > 0.10$) between identified compounds and C-CH_4 production potentials at the 3 °C incubation temperature (b).

sediment deposition and following perennial freezeup of sediment (i.e., permafrost formation), in influencing the high proportions of biolabile OM found in yedoma permafrost sediments.

During our 154-day anaerobic incubation, the relative abundance of condensed aromatic, polyphenolic, and peptide-like compounds increased and the relative abundance of unsaturated high oxygen and aliphatic compounds decreased (Figures 3 and 4). The decreasing relative abundance of unsaturated high oxygen and aliphatic compounds are most likely resultant of these compounds being preferentially mineralized, while the increasing abundance of condensed aromatic, polyphenolic, and peptide-like compounds reflect OM conservation and/or production. This is consistent with prior findings in aerobic arctic aquatic ecosystems, where the aliphatic fractions of permafrost OM had rapid, high rates of degradation (83%) during a 28-day aerobic incubation (Spencer et al., 2015). We note that, at the 12-m depth, the relative abundance of condensed aromatic compounds decreased and the relative abundance of unsaturated high oxygen compounds increased during our anaerobic incubation. We attribute these differences to microbial communities at our deepest sampled yedoma depth utilizing different metabolic pathways (Mackelprang et al., 2017), and further discuss these results in section 4.4.

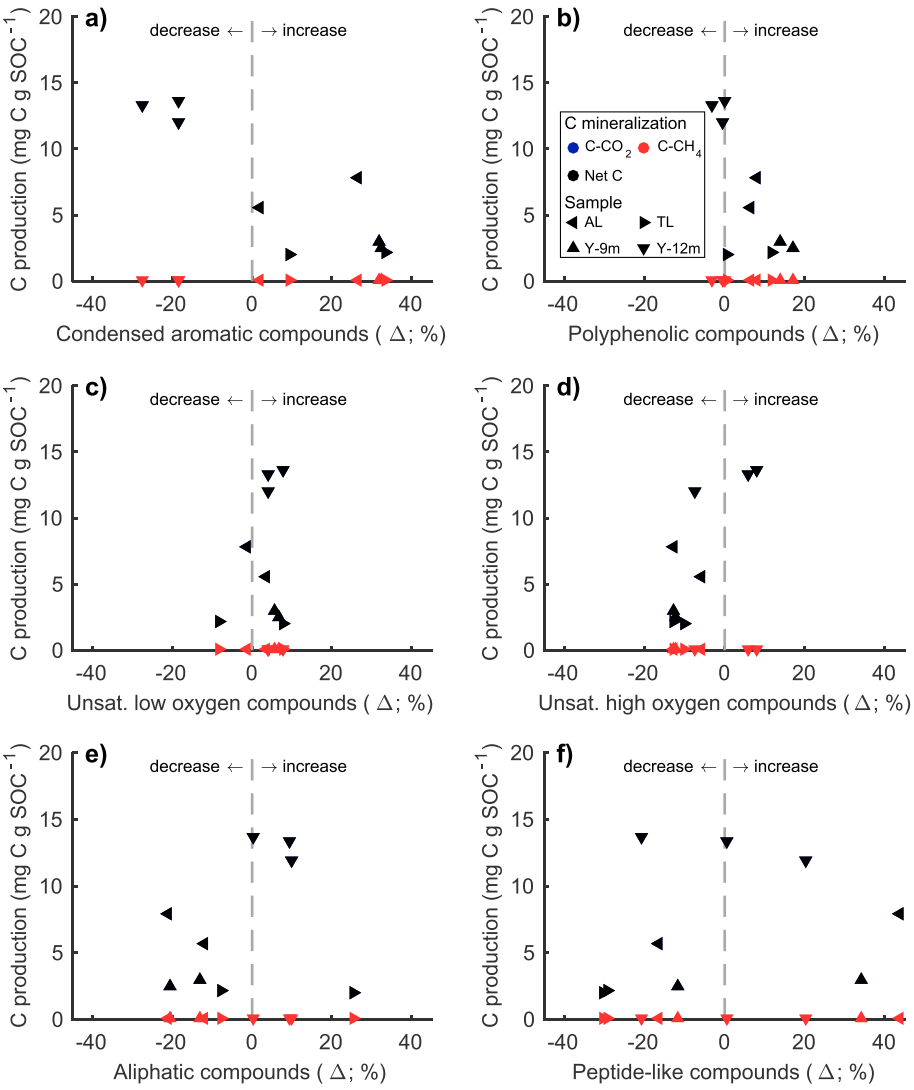

Figure 3. Changes in relative abundance of WEOM compound classes versus C mineralization during a 154-day anaerobic incubation at the 3 °C incubation temperature.

4.2. Microbial Community Characteristics

Our results show that the VC permafrost profile contains viable microbial communities adapted to a deep permafrost environment with no new OC or energy inputs during the millennia since permafrost formation. We observed changing microbial communities and decreasing bacterial diversity, but relatively consistent archaeal diversity, with increasing depth in the VC permafrost tunnel (Figure 5). Increased bacterial diversity in the AL and TL horizons may be due to prior thawing allowing the reintroduction of energy and biolabile substrates in these near-surface horizons. Unlike in the deeper yedoma horizons, which have remained constantly frozen since their formation approximately 45,000 years ago (Schirrmeister et al., 2016), soils in the AL currently experience seasonal freezing and thawing, and the TL horizon is comprised of yedoma soils which thawed approximately 5,000–7,000 years ago during the Holocene thermal optimum, subsequently refroze, and remained frozen until the present (Schirrmeister et al., 2013). Since microbial communities in the AL and TL horizons may have received fresh substrate during thawed periods and would not have been forced to adapt their metabolisms due to substrate limitations, we propose that bacterial communities were able to maintain higher diversity (higher Inverse Simpson Indices; Figure 5a) to fill a greater range of metabolic niches.

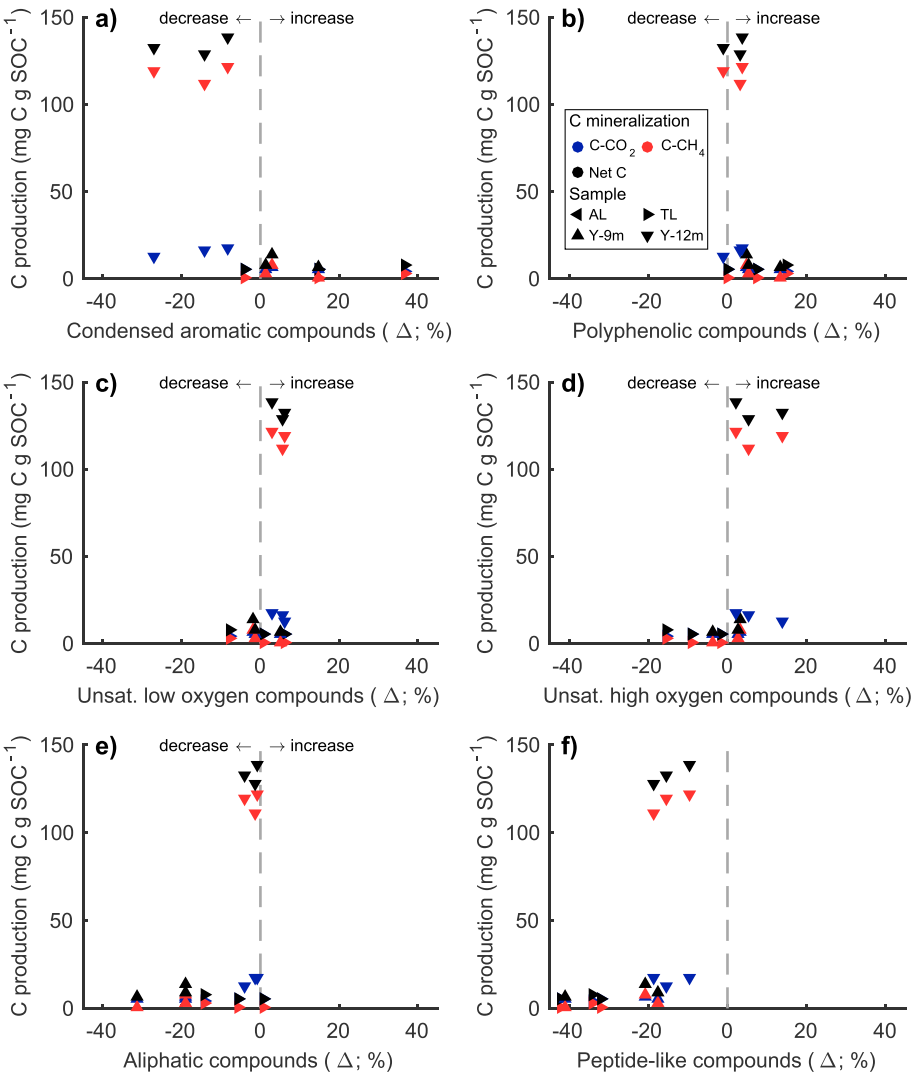

Figure 4. Changes in relative abundance of WEOM compound classes versus C mineralization during a 154-day anaerobic incubation at the 13 °C incubation temperature.

Compared to other regions, few studies examine microbial diversity in Arctic soils (Malard & Pearce, 2018); most of these studies examine microbial communities in the modern active layer, and few studies have characterized microbes in deeper permafrost. At the circumarctic scale, active layer soil bacterial communities are dominated by *Rhizobiales*, *Burkholderiales*, *Xanthomonadales*, and *Myxococcales* (Malard & Pearce, 2018). We detected each of these taxa in the modern active layer but, with the exception of *Burkholderiales*, not in the deeper permafrost samples. Permafrost soil bacterial communities at the VC permafrost tunnel were dominated by *Burkholderiales* (*Proteobacteria*/*Betaproteobacteria*; 62.0% relative abundance in the TL sample), *Campylobacterales* (*Proteobacteria*/*Epsilonproteobacteria*; 54.9% relative abundance in the Y-9m sample), and *Micrococcales* (*Actinobacteria*; 29.1% and 99.7% relative abundance in the Y-9m and Y-12m samples, respectively). Yedoma permafrost samples from the U.S. Army Cold Regions and Research and Engineering Laboratory (CRREL) permafrost tunnel, located ~10 km south of the VC permafrost tunnel, were also dominated by *Actinobacteria*, *Proteobacteria*, and *Bacteroidetes* (Mackelprang et al., 2017). Relative abundance of *Proteobacteria* decreased with age/depth at both the CRREL and VC permafrost tunnels (Mackelprang et al., 2017). However, while Mackelprang et al. (2017) observed decreasing relative abundance of *Actinobacteria* with increasing permafrost age at the CRREL permafrost tunnel, we observed increasing relative abundance of *Actinobacteria* (up to 99.7% at 12-m

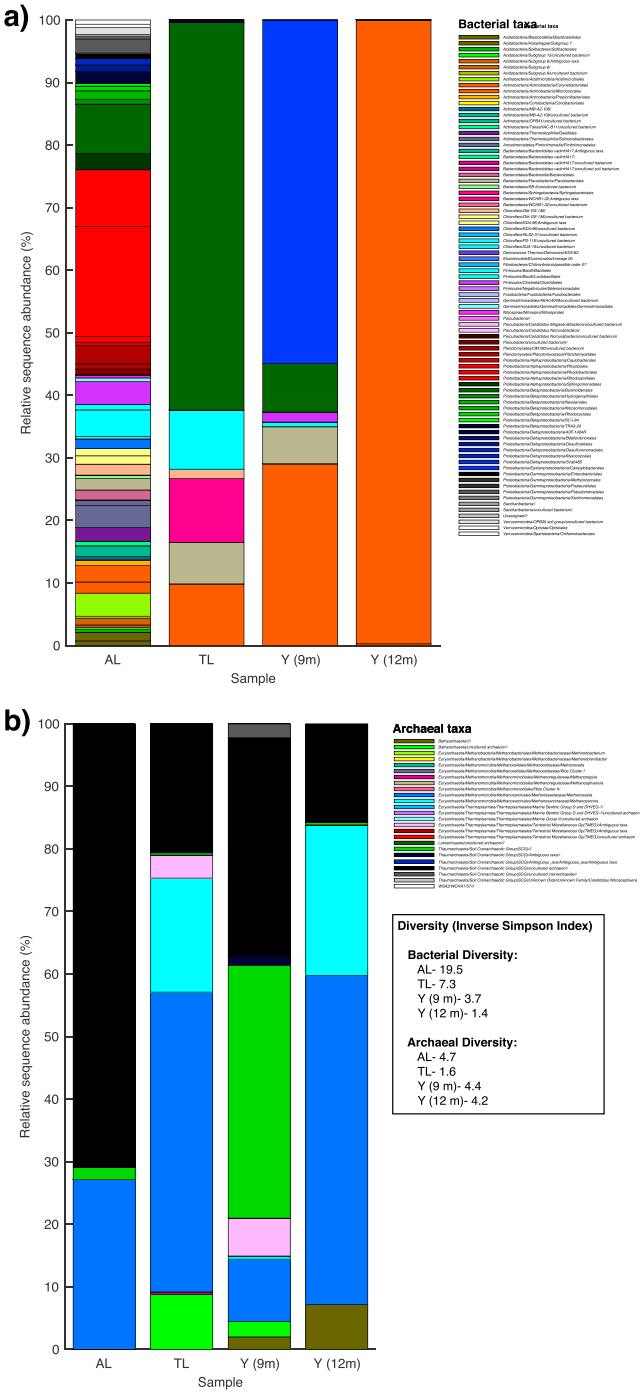

Figure 5. Relative sequence abundance of (a) bacterial and (b) archaeal 16S rRNA genes in sediments from four depths in the VC permafrost tunnel, measured prior to incubation. We report bacterial and archaeal diversity at each sample depth using the Inverse Simpson Index; values are stated below each sample name.

depth) with increasing depth in the VC permafrost tunnel. We also observed decreasing relative abundance of *Firmicutes* with increasing depth in the VC permafrost tunnel, as opposed to increasing relative abundance with increasing permafrost age in the CRREL permafrost tunnel (Mackelprang et al., 2017).

Prior studies have demonstrated that microbes in permafrost perform metabolic processes, grow, and divide (Mackelprang et al., 2017; Rivkina et al., 2000; Wagner et al., 2007; Waldrop et al., 2010), albeit at slower rates than in nonfrozen soils. These active microbial communities in permafrost demonstrate a long-term microbial survival strategy, as microbial metabolic activity is preferable to dormancy for preserving DNA (Dieser et al., 2013; Willerslev et al., 2004). Over geologic (millennial) time scales, limited resources and substrate would be available for microbial communities in the undisturbed yedoma permafrost and, due to buried and frozen conditions, no new OC input would have been received, forcing microbial metabolism to adapt to consume normally stable fractions of OM (Mackelprang et al., 2017). We see potential evidence of microbial communities adapting to resource limitations in the bacterial abundance data, which show an increase in *Actinobacteria* (order *Micrococcales*, genus *Arthrobacter*) with depth (Figure 5). *Actinobacteria* were detected at all sampled depths in the VC permafrost tunnel, and increased in relative abundance with depth, up to 99.7% bacterial abundance at the 12-m depth. *Actinobacteria* are known to degrade aromatic compounds even under anaerobic conditions (Busse et al., 2015). The increasing relative abundance of *Actinobacteria* coupled with decreasing relative abundance of condensed aromatic compounds with depth suggests that in situ bacterial communities under energy-limited conditions may have been forced to adapt to metabolize normally stable fractions of WEOM.

Archaeal diversity may not be as strongly influenced by sediment age as bacterial diversity due to archaeal capacity to better withstand extreme conditions. At the VC permafrost tunnel, archaeal diversity was dominated by the Soil Crenarchaeotic Group (SCG; *Thaumarchaeota*; up to 70.9% relative abundance) and *Methanosarcinales* (up to 52.6% relative abundance). Prior studies have also found large abundances of *Methanomicrobia* in Alaskan soils (Malard & Pearce, 2018). Methanogens have also been detected in buried yedoma permafrost in northeast Russian (Bischoff et al., 2013; Rivkina et al., 1998) and the CRREL permafrost tunnel in Fox, AL (Mackelprang et al., 2017). In the CRREL permafrost tunnel, methanogen relative abundance decreased with increasing permafrost age (Mackelprang et al., 2017), while in our study at the VC permafrost tunnel methanogen relative abundance did not significantly change with depth. The identification of methanogens in buried, previously undisturbed yedoma is important because, following permafrost thaw, stable methanogen communities are necessary to metabolize permafrost OC into CH_4 (Knoblauch et al., 2018). Prior to the establishment of stable CH_4-producing microbial communities, GHG emissions from thawed permafrost OC are dominated by CO_2 (Knoblauch et al., 2018; Schädel et al., 2016); however, following the establishment of these communities over longer times, permafrost OC mineralized under anaerobic conditions has the potential to emit equal quantities of CO_2 and CH_4 (Knoblauch et al., 2018). Methanogens of the taxa *Methanosarcinales*, which we detected at all our sampled depths (Figure 5b), have been previously associated with rapid increases in number and subsequent CH_4 emissions following permafrost thaw (Wei et al., 2018). Therefore, the detection of methanogens at all

sampled depths in the VC permafrost tunnel suggests that in situ microbial communities in this yedoma profile, including deep yedoma, are equipped to metabolize OM into CH_4 following thaw.

4.3. Potential C Mineralization Following Thaw

We found increasing anaerobic GHG production potentials (C-CO_2, C-CH_4, and net C; Table 2 and Figures S1 and S2), decreasing C-CO_2:C-CH_4 ratios, and increasing temperature sensitivities (Q_{10}; Table 2) with depth in the perennial frozen permafrost samples (TL, Y-9m, and Y-12m) from the VC permafrost tunnel. C-CO_2 and net C production potentials were higher in the modern AL than in the underlying TL sample. While yedoma OC has been previously shown to be highly biolabile upon thaw (Dutta et al., 2006; Knoblauch et al., 2013, 2018; Vonk et al., 2013), our results demonstrate that GHG production from thawing yedoma permafrost OC increases with depth. Our results suggest that OC from thawed yedoma sediments will produce more GHG per unit OC as permafrost thaw depths increase (4.1 times more GHG production at 12- versus 9-m depth at 3 °C and 9.9 times more GHG production at 13 °C).

C-CO_2:C-CH_4 ratios generally decreased with depth, and the yedoma permafrost samples (Y-9m and Y-12m) produced more CH_4 than CO_2 during our 154-day incubation at 13 °C (Figures S1 and S2 and Table 2). While we did not measure pH as part of this study, higher $C_{inorganic}$ content in the yedoma permafrost samples (Table 1) may be indicative of slightly higher pH in our incubated slurries from these depths. In a Siberian yedoma permafrost profile, pore ice from depths with comparable sediment $C_{inorganic}$ content to our Y-9m and Y-12m samples were pH 8.0–8.5, as opposed to pH ~8 at depths with sediment $C_{inorganic}$ content comparable to the AL and TL horizons in our study (Schirrmeister et al., 2017). The potentially higher slurry pH at the Y-9m and Y-12m depths in the VC permafrost tunnel may contribute to an underestimation of CO_2 production at these depths, given that our calculations and comparisons assume consistent pH at all depths. Nevertheless, our results still indicate that, with increasing depth, greater proportions of C were mineralized as CH_4 versus CO_2 during anaerobic incubation. We primarily attribute these changing C-CO_2:C-CH_4 ratios to depth-related changes in both substrate potential and in situ microbial communities, which we further discuss in section 4.4. Given that CH_4 has 34 times more GWP than CO_2 over a 100-year time scale (Schädel et al., 2016), these results indicate that C mineralization has increasing GWP with deeper thaw depths in yedoma permafrost. Thawed yedoma sediments in our study had 2 times higher GWP at 12- versus 9-m depth at 3 °C and 15 times higher GWP at 13 °C (Figure 6).

Increasing Q_{10} values with depth in our incubation (Table 2) further suggest that deeper yedoma OM is more sensitive to warming, and C mineralization of OM from these deeper depths will show a greater temperature response following thaw and remobilization. Temperature is known to be a primary control on both C mineralization rates (Conant et al., 2011; Schädel et al., 2016) and the amount of DOM leached from soils (O'Donnell et al., 2016). At warmer temperatures, we observe higher C mineralization rates and more DOM release from soils. Our results from the VC permafrost tunnel show that the magnitude of C mineralization increase (Q_{10}) between 3 and 13 °C, two temperatures found in thermokarst lake sediments (Heslop et al., 2015), increases with thaw depth. We hypothesize that the increasing Q_{10} values with depth are due to a combination of the deeper yedoma permafrost leaching more, higher-quality WEOM substrate and a rapid bloom in microbial community biomass following warming. We further discuss these potential relationships between substrate quality, microbial communities, and GHG production in the following section.

4.4. Relationships Between OM, Microbial Communities, and C Mineralization

With the exception of C-CH_4 production at the 3 °C incubation temperature, anaerobic C mineralization (C-CO_2, C-CH_4, and net C) at both incubation temperatures (3 and 13 °C) negatively correlated with C_{org}:N_{tot} ratios and positively correlated with total Fe. The negative correlation between anaerobic C mineralization and C_{org}:N_{tot} ratios is expected given that lower C_{org}:N_{tot} ratios are indicative of less degraded OM. It is well established that Fe is the most abundant metal utilized in enzymatic pathways for methanogenesis (Glass and Orphan, 2012) and CH_4 production positively correlates to Fe (III):total Fe ratios in anaerobic environments (Herndon et al., 2015). While total Fe concentrations positively correlated with C mineralization in our anaerobic environments, we note that we did not measure Fe oxidation state and oxidized Fe can stabilize and aid in sequestering OM (Salvadó et al., 2015; Vermeire et al., 2019).

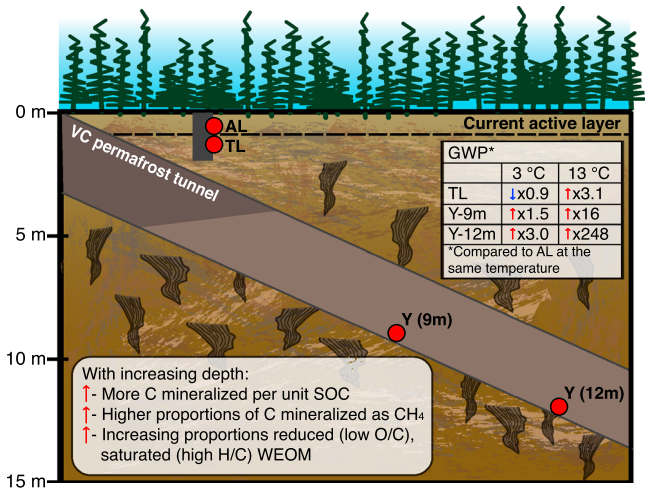

Figure 6. Schematic diagram of sampling at the VC permafrost tunnel with key findings summarized.

We suggest that the changes in WEOM composition (increasing aliphatic and peptide-like contributions and decreasing condensed aromatic relative abundance with depth) we observed in our profile could potentially be indicative of long-term WEOM processing and conservation in the reduced, yedoma-type permafrost. While we did not analyze microbial metabolic pathways as part of this study, it is possible that the decrease in the relative abundance of condensed aromatic compounds observed during our anaerobic incubation at the 12-m depth may be associated with *Actinobacteria* (Busse et al., 2015) and/or *Bathyarchaeota* (Xiang et al., 2017). *Actinobacteria* were detected at all sampled depths (9.9–99.7% bacteria relative abundance; Figure 5a) and represented 99.7% of bacteria relative abundance in the Y-12m sample, and we detected *Bathyarchaeota* in the perennially frozen permafrost (4.7–8.8% archaea relative abundance; Figure 5b). *Actinobacteria* are known to degrade aromatic compounds even under anaerobic conditions (Busse et al., 2015), while *Bathyarchaeota* have been associated with fermentation of organic substrates and degradation of aromatic compounds (Xiang et al., 2017). In the CRREL permafrost tunnel, older yedoma permafrost was found to have increased capacity for degrading aromatic hydrocarbons to benzoyl-CoA (Mackelprang et al., 2017), which in turn could be anaerobically fermented into acetate using CO_2 (Fuchs, 2008). Acetate, in turn, can be directly utilized as substrate by acetoclastic methanogens (*Methanosarcina* and *Methanosaeta*; 24.0% and 52.6% relative abundance, respectively, in the Y-12m sample), contributing to the high CH_4 production we observed at this sample depth. This is consistent with high acetate concentrations in deep yedoma permafrost observed by Drake et al. (2015) and Ewing et al. (2015), coupled with rapid acetate depletion following thaw (Drake et al., 2015). Over longer periods of time, we anticipate that CO_2:CH_4 production ratios in our incubation would stabilize to 1:1 (Knoblauch et al., 2018).

Bathyarchaeota metabolisms have also been linked to enriched amino acids and peptides in deep-sea floor sediments which, like yedoma permafrost, are cold, anoxic, energy-limited environments (Lloyd et al., 2013). This may, in part, account for the increased relative abundance of peptide-like compounds we observed with depth in the VC permafrost tunnel (Figure 1). In the CRREL permafrost tunnel, amino acid and peptide metabolic pathways were enriched in the older yedoma permafrost (Mackelprang et al., 2017), suggestive of biomass recycling being a source of microbial substrate over time scales of thousands of years (Lloyd et al., 2013; Mackelprang et al., 2017). Given the millennia (approximately 45,000 years; Schirrmeister et al., 2016) since permafrost formation at our sampled depths in the VC permafrost tunnel, these metabolic processes could potentially contribute to the increased relative abundance of peptide-like compounds with increasing depth.

Initial relative abundance of aliphatic compounds positively correlated with CO_2 production (3 and 13 °C), CH_4 production (13 °C), and net C production (3 and 13 °C) in our anaerobic incubations (Table S1). The decreasing relative abundances we observed for aliphatic compounds at all depths and incubation temperatures except Y-12m at 3 °C (Figures 3e and 4e) suggest that these compounds are preferentially mineralized into GHG following permafrost thaw. Aliphatic compounds have been previously shown to have high substrate potential for GHG production and be rapidly degraded following permafrost thaw (Drake et al., 2018; Spencer et al., 2015; Stapel et al., 2016, 2017). Thus, increasing abundance of aliphatic compounds in yedoma permafrost with depth (this study; Ewing et al., 2015; Stapel et al., 2016, 2017) suggests increasing OC quality and, by extension, increasing anaerobic C mineralization potentials per unit OC with depth.

Anaerobic CO_2 production in our incubations also negatively correlated with initial relative abundance of unsaturated high and low oxygen compounds (Figure 2 and Table S1). With the exception of the Y-12m depth, relative abundance of unsaturated high oxygen compounds decreased during our anaerobic incubations (Figures 3d and 4d). We hypothesize that microbial communities in our anaerobic incubations are utilizing oxygen from these compounds to produce CO_2 as an intermediate step in methanogenesis. At all depths except the Y-12m depth, we detected bacteria of the orders *Bacteroidales* and *Clostridales* in our initial microbial communities (Figure 5a). These bacteria are known to ferment complex organic matter into

acetate, H_2, and CO_2 (Rojas et al., 2018), and have been previously shown to co-occur with methanogens in environments with degraded OM (Baldwin et al., 2015). Given that this fermentation of complex OM into substrate for methanogenesis is the rate-limiting step in Arctic anaerobic C mineralization (Zheng et al., 2019), it is possible that the degradation of unsaturated high oxygen compounds we observed in our anaerobic incubation correlates to fermentation of OM by *Bacteroidales* and *Clostridales* into substrate for methanogenesis.

We attribute decreasing C-CO_2:C-CH_4 ratios with depth to depth-related changes in both substrate potential and in situ microbial communities. Changes in anaerobic C-CO_2:C-CH_4 ratios have also been previously linked to changes in microbial community composition and respective microbial metabolisms in wetland environments (Juottonen et al., 2017). As discussed above, increasing proportions of aliphatic WEOM compounds with depth indicate increasing proportions of energy-rich potential substrate that can be utilized by methanogens and mineralized into CH_4. Additionally, in conjunction with higher microbial diversity at our shallower sampled depths (AL and TL horizons), we detected higher abundances of taxa that mineralize C into CO_2 instead of CH_4.

4.5. Ramifications for the Permafrost Carbon Feedback

While previous studies have shown that high proportions of OC in yedoma permafrost are bioavailable upon thaw, our observed changes in yedoma WEOM composition and anaerobic C mineralization potentials with depth due to long-term processing and conservation under reduced, anaerobic conditions need to be taken into consideration when estimating the role of thawed yedoma OC in the PCF. Aliphatic compounds, which increased in relative abundance with depth in the VC permafrost tunnel, were preferentially mineralized during our anaerobic incubations, and samples with higher abundances of aliphatic compounds produced more GHG and higher proportions of CH_4 (indicated by lower C-CO_2:C-CH_4 ratios). However, we also note different trends in WEOM utilization at Y-12m depth, which we attribute to microbial communities at this depth utilizing different metabolic pathways. We suggest that the high relative abundance of *Actinobacteria* (99.7% bacterial relative abundance) and *Bathyarchaeota* (7.2% archaeal relative abundance) indicate increased microbial capacity to anaerobically ferment aromatic hydrocarbons, which are normally stable compounds, to benzoyl-CoA, which can be subsequently metabolized into acetate and utilized by *Methanosarcina* and *Methanosaeta* to produce CH_4. Combined, these findings highlight the disproportionately important contribution of thawing deep yedoma OC in potential GHG, and especially CH_4, emissions from thawing permafrost.

Considering that yedoma-type permafrost is particularly vulnerable to thermokarst and thermoerosional processes (Schneider von Deimling et al., 2015), which rapidly thaw and mobilize deep permafrost OC, it is crucially important to account for this increasing GHG production and GWP per unit OC with depth to better understand how the release of thawed ancient OC from deep yedoma permafrost will impact the magnitude of the PCF and global C cycling. Permafrost thaw and subsequent permafrost OC mineralization from these rapid, deep thaw processes release substantially more ^{14}C-depleted GHG than other permafrost thaw mechanisms such as active layer deepening (Walter Anthony et al., 2018), and are not yet accounted for in land models estimating the magnitude of the PCF (Burke et al., 2017; Koven et al., 2013, 2015; McGuire et al., 2018; Schaefer et al., 2014). Given our findings that the GWP of mineralized yedoma OC increases with depth (Figure 6 and Table 2), accounting for these thaw processes becomes even more critical in estimating the potential magnitude of the PCF.

Acknowledgments
We thank P. Anthony, S. Billings, J. Chanton, J. Guerard, N. Haubenstock, F. Horn, T. Howe, C. Knoblauch, L. Oliver, A. Saborowski, and B. Van Veldhuizen for their assistance in data collection and/or analysis and S. Skidmore for granting access to the Vault Creek permafrost tunnel. Funding for FT-ICR MS facilities at the NHMFL was provided by NSF DMR-1157490. Additional funding for J. Heslop has been provided by the Department of Geography and Planning at Queen's University, the University of Alaska Fairbanks (UAF) Graduate School, a UAF Center for Global Change Student Research Grant with funds from the UAF Center for Global Change, and STAR Fellowship Assistance agreement FP-91762901-0 awarded by the U.S. Environmental Protection Agency (EPA). This manuscript has not been formally reviewed by EPA. The views expressed in this presentation are solely those of J. Heslop, and the EPA does not endorse any products or commercial services mentioned. K.M. Walter Anthony was supported by NSF ARC-1304823 and NASA ABoVE NNX15AU49A. M. Winkel was supported by the NSF ARCSS-1500931. S. Liebner was supported by the Helmholtz Young Investigators Group of S.L. (VH-NG-919). Microbial sequence data have been deposited at NCBI under the Bioproject PRJNA432510 (www.ncbi.nlm.nih.gov/bioproject/?term=PRJNA432510) with the sequence read archive accession numbers SRR6740235, SRR6740237, SRR6740232, and SRR6740246 for bacterial and SRR6729506, SRR6729504, SRR6729509, and SRR6729533 for archaeal sequences, respectively. All geochemistry, WEOM composition, and incubation data summarized in the figures and tables can be found in Data Set S1 in the supporting information.

References

Adam, P. S. (2017). The growing tree of Archaea: New perspectives on their diversity, evolution and ecology. *ISME Journal*. *11*(11), 2407–2425. https://doi.org/10.1038/ismej.2017.122

Baldwin, S. A., Khoshnoodi, M., Rezadehbashi, M., Taupp, M., Hallam, S., Mattes, A., & Sanei, H. (2015). The microbial community of a passive biochemical reactor treating arsenic, zinc, and sulfate-rich seepage. *Frontiers in Bioengineering and Biotechnology*, *3*. https://doi.org/10.3339/fbioe.2015.00027

Bischoff, J., Mangelsdorf, K., Gattinger, A., Schloter, M., Kurchatova, A. N., Herzschuh, U., & Wagner, D. (2013). Response of methanogenic archaea to late Pleistocene and Holocene climate changes in the Siberian Arctic. *Global Biogeochemical Cycles*, *27*, 305–317. https://doi.org/10.1029/2011GB004238

Bolger, A. M., Lohse, M., & Usadel, B. (2014). Trimmomatic:A flexible trimmer for Illumina sequence data. *Bioinformatics*, *30*(15), 2114–2120. https://doi.org/10.1093/bioinformatics/btu170

Burke, E. J., Ekici, A., Huang, Y., Chadburn, S. E., Huntingford, C., Ciais, P., et al. (2017). Quantifying uncertainties of permafrost carbon-climate feedbacks. *Biogeoscience*, *14*(12), 3051–3066. https://doi.org/10.5194/bg-14-3051-2017

Busse, H.-J., Wieser, M., & Buczolits, S. (2015). Arthrobacter. In *Bergey's Manual of Systematics of Archaea and Bacteria*. John Wiley & Sons, Ltd. https://doi.org/10.1002/9781118960608.gbm00118

Caporaso, J. G., Kuczynski, J., Stombaugh, J., Bittinger, K., Bushman, F. D., Costello, E. K., et al. (2010). QIIME allows analysis of high-throughput community sequencing data. *Nature Methods*, *7*(5), 335–336. https://doi.org/10.1038/nmeth.f.303

Castelle, C. J., Wrighton, K. C., Thomas, B. C., Hug, L. A., Brown, C. T., Wilkins, M. J., et al. (2015). Genomic expansion of domain archaea highlights roles for organisms from new phyla in anaerobic carbon cycling. *Current Biology*, *25*(6), 690–701. https://doi.org/10.1016/j.cub.2015.01.014

Comyn-Platt, E., Hayman, G., Huntingford, C., Chadburn, S. E., Burke, E. J., Harper, A. B., et al. (2018). Carbon budgets for 1.5 and 2 °C targets lowered by natural wetland and permafrost feedbacks. *Nature Geoscience*, *11*(8), 568–573. https://doi.org/10.1038/s41561-018-0174-9

Conant, R. T., Ryan, M. G., Ågren, G. I., Birge, H. E., Davidson, E. A., Eliasson, P. E., et al. (2011). Temperature and soil organic matter decomposition rates—Synthesis of current knowledge and a way forward. *Global Change Biology*, *17*(11), 3392–3404. https://doi.org/10.1111/j.1365-2486.2011.02496.x

Corilo Y., EnviroOrg. Florida State University, 2015.

Dieser, M., Battista, J. R., & Christner, B. C. (2013). DNA double-strand break repair at −15 °C. *Applied and Environmental Microbiology*, *79*(24), 7662–7668. https://doi.org/10.1128/AEM.02845-13

Dittmar, T., Koch, B., Hertkorn, N., & Kattner, G. (2008). A simple and efficient method for the solid-phase extraction of dissolved organic matter (SPE-DOM) from seawater. *Limnology and Oceanography: Methods*, *6*, 230–235. https://doi.org/10.4319/lom.2008.230

Drake, T. W., Guillemette, F., Hemingway, J. D., Chanton, J. P., Podgorski, D. C., Zimov, N. S., & Spencer, R. G. M. (2018). The Ephemeral signature of permafrost carbon in an arctic fluvial network. *Journal of Geophysical Research: Biogeosciences*, *123*, 1475–1485. https://doi.org/10.1029/2017JG004311

Drake, T. W., Wickland, K. P., Spencer, R. G. M., McKnight, D. M., & Striegl, R. G. (2015). Ancient low-molecular-weight organic acids in permafrost fuel rapid carbon dioxide production upon thaw. *Proceedings of the National Academy of Sciences*, *112*(45), 13,946–13,951. https://doi.org/10.1073/pnas.1511705112

Dutta, K., Schuur, E. A. G., Neff, J. C., & Zimov, S. A. (2006). Potential carbon release from permafrost soils of northeastern Siberia. *Global Change Biology*, *12*(12), 2336–2351. https://doi.org/10.1111/j.1365-2486.2006.01259.x

Ewing, S. A., O'Donnell, J. A., Aiken, G. R., Butler, K., Butman, D., Windham-Myers, L., & Kanevskiy, M. Z. (2015). Long-term anoxia and release of ancient, labile carbon upon thaw of Pleistocene permafrost. *Geophysical Research Letters*, *42*, 10,730–10,738. https://doi.org/10.1002/2015GL066296

Fuchs, G. (2008). Anaerobic metabolism of aromatic compounds. *Annals of the New York Academy of Sciences*, *1125*(1), 82–99. https://doi.org/10.1196/annals.1419.010

Glass and Orphan (2012). Trace metal requirements for microbial enzymes involved in the production and consumption of methane and nitrous oxide. *Frontiers in Microbiology*, *3*(61). https://doi.org/10.3389/fmicb.2012.00061

Graham, D. E., Wallenstein, M. D., Vishnivetskaya, T. A., Waldrop, M. P., Phelps, T. J., Pfiffner, S. M., et al. (2012). Microbes in thawing permafrost: The unknown variable in the climate change equation. *The ISME Journal*, *6*(4), 709–712. https://doi.org/10.1038/ismej.2011.163

Haney, R. L., Franzluebbers, A. J., Jin, V. L., Johnson, M. V., Haney, E. B., White, M. J., & Harmel, R. D. (2012). Soil organic C:N vs. water-extractable organic C:N. *Open Journal of Soil Science*, *02*(03), 269–274. https://doi.org/10.4236/ojss.2012.23032

Herlemann, D. P., Labrenz, M., Jürgens, K., Bertilsson, S., Waniek, J. J., & Andersson, A. F. (2011). Transitions in bacterial communities along the 2000 km salinity gradient of the Baltic Sea. *ISME Journal*, *5*(10), 1571–1579. https://doi.org/10.1038/ismej.2011.41

Herndon, E. M., Yang, Z., Bargar, J., Janot, N., Regier, T. Z., Graham, D. E., et al. (2015). Geochemical drivers of organic matter decomposition in arctic tundra soils. *Biogeochemistry*, *126*(3), 397–414. https://doi.org/10.1007/s10533-015-0165-5

Heslop, J. K., Walter Anthony, K. M., Sepulveda-Jauregui, A., Martinez-Cruz, K., Bondurant, A., Grosse, G., & Jones, M. C. (2015). Thermokarst lake methanogenesis along a complete talik profile. *Biogeosciences*, *12*(14), 4317–4331. https://doi.org/10.5194/bg-12-4317-2015

Jorgenson, T., Yoshikawa, K., Kanevskiy, M., Shur, Y., Romanovsky, V., Marchenko, S., et al. (2008). *Permafrost characteristics of Alaska. Proceedings of the Ninth International Conference on Permafrost* (pp. 121–122). Fairbanks, AK: University of Alaska Fairbanks. 29 June to 03 July, 2008.

Juottonen et al (2017). Distinct anaerobic bacterial consumers of cellobiose-derived carbon in boreal fens differing in CH4 vs. CO2 production ratio. *Applied and Environmental Microbiology*, *83*(4). https://doi.org/10.1128/AEM.02533-16

Kaiser, N. K., Quinn, J. P., Blakney, G. T., Hendrickson, C. L., & Marshall, A. G. (2011). A novel 9.4 tesla FTICR mass spectrometer with improved sensitivity, mass resolution, and mass range. *Journal of the American Society for Mass Spectrometry*, *22*(8), 1343–1351. https://doi.org/10.1007/s13361-011-0141-9

Kanevskiy, M., Shur, Y., Fortier, D., Jorgenson, M. T., & Stephani, E. (2011). Cryostratigraphy of late Pleistocene syngenetic permafrost (yedoma) in northern Alaska, Itkillik River exposure. *Qualitative Research*, *75*(3), 584–596. https://doi.org/10.1016/j.yqres.2010.12.003

Kanevskiy, M., Shur, Y., Strauss, J., Jorgenson, T., Fortier, D., Stephani, E., & Vasiliev, A. (2016). Patterns and rates of riverbank erosion involving ice-rich permafrost (yedoma) in northern Alaska. *Geomorphology*, *253*, 370–384. https://doi.org/10.1016/j.geomorph.2015.10.023

Kessler, M. A., Plug, L. J., & Walter Anthony, K. M. (2012). Simulating the decadal- to millennial-scale dynamics of morphology and sequestered carbon mobilization of two thermokarst lakes in NW Alaska. *Journal of Geophysical Research*, *117*, G00M06. https://doi.org/10.1029/2011JG001796

Knoblauch, C., Beer, C., Liebner, S., Grigoriev, M. N., & Pfeiffer, E. M. (2018). Methane production as key to the greenhouse gas budget of thawing permafrost. *Nature Climate Change*, *8*(4), 309–312. https://doi.org/10.1038/s41558-018-0095-z

Knoblauch, C., Beer, C., Sosnin, A., Wagner, D., & Pfeiffer, E. M. (2013). Predicting long-term carbon mineralization and trace gas production from thawing permafrost of Northeast Siberia. *Global Change Biology*, *19*(4), 1160–1172. https://doi.org/10.1111/gcb.12116

Koch, B. P., & Dittmar, T. (2006). From mass to structure: An aromaticity index for high-resolution mass data of natural organic matter. *Rapid Communications in Mass Spectrometry*, *20*(5), 926–932. https://doi.org/10.1002/rcm.2386

Koch, B. P., Dittmar, T., Witt, M., & Kattner, G. (2007). Fundamentals of molecular formula assignment to ultrahigh resolution mass data of natural organic matter. *Analytical Chemistry*, *79*, 1758–1763. https://doi.org/10.1021/ac061949s

Koven, C. D., Lawrence, D. M., & Riley, W. J. (2013). Permafrost carbon-climate feedback is sensitive to deep soil carbon decomposability but not deep soil nitrogen dynamics. *Proceedings of the National Academy of Sciences*, *112*, 3752–3757.

Koven, C. D., Schuur, E. A. G., Schädel, C., Bohn, T. J., Burke, E. J., Chen, G., et al. (2015). A simplified, data-constrained approach to estimate the permafrost carbon–climate feedback. *Philosophical Transactions of the Royal Society A*, *373*(2054). https://doi.org/10.1098/rsta.2014.0423

Lenton, T. (2012). Arctic climate tipping points. *Ambio*, *41*(1), 10–22. https://doi.org/10.1007/s13280-011-0221-x

Lloyd, K. G., Schreiber, L., Petersen, D. G., Kjeldsen, K. U., Lever, M. A., Steen, A. D., et al. (2013). Predominant archaea in marine sediments degrade detrital proteins. *Nature*, *496*(7444), 215–218. https://doi.org/10.1038/nature12033

Mackelprang, R., Burkert, A., Haw, M., Mahendrarajah, T., Conaway, C. H., Douglas, T. A., & Waldrop, M. P. (2017). Microbial survival strategies in ancient permafrost: Insights from metagenomics. *The ISME Journal*, *11*(10), 2305–2318. https://doi.org/10.1038/ismej.2017.93

Mackelprang, R., Waldrop, M. P., DeAngelis, K. M., David, M. M., Chavarria, K. L., Blazewicz, S. J., et al. (2011). Metagenomic analysis of a permafrost microbial community reveals a rapid response to thaw. *Nature*, *480*(7377), 368–371. https://doi.org/10.1038/nature10576

Malard, L., & Pearce, D. (2018). Microbial diversity and biogeography in Arctic soils. *Environmental Microbiology Reports*, *10*(6), 611–625. https://doi.org/10.1111/1758-2229.12680

Mann, P. J., Sobczak, W. V., LaRue, M. M., Bulygina, E., Davydova, A., Vonk, J. E., et al. (2014). Evidence for key enzymatic controls on metabolism of Arctic river organic matter. *Global Change Biology*, *20*(4), 1089–1100. https://doi.org/10.1111/gcb.12416

Martin, M. (2011). Cutadapt removes adapter sequences from high-throughput sequencing reads. *EMBnet.journal*, *17*(1), 10–12. https://doi.org/10.14806/ej.17.1.200

McGuire, A. D., Lawrence, D. M., Koven, C., Clein, J. S., Burke, E., Chen, G., et al. (2018). Dependence of the evolution of carbon dynamics in the northern permafrost region on the trajectory of climate change. *Proceedings of the National Academy of Sciences*, *115*(15), 3882–3887. https://doi.org/10.1073/pnas.1719903115

Meyer, H., Yoshikawa, K., Schirrmeister, L., & Andreev, A. (2008). The Vault Creek Tunnel (Fairbanks Region, Alaska): A lQuaternary palaeoenvironmental permafrost record. Proceedings of the Ninth International Conference on Permafrost, 1191–1196, University of Alaska Fairbanks, Fairbanks, Alaska, USA, 29 June to 03 July, 2008.

Myhre G., Shindell, D., Bréon, F. M., Collins, W., Fuglestvedt, J., Huang, J., et al. (2013). Anthropogenic and natural radiative forcing, climate change 2013: The physical science basis. Contribution of Working Group I to the Fifth Assessment Report of the Intergovernmental Panel on Climate Change. Intergovernmental Panel on Climate Change, New York, USA.

O'Donnell, J. A., Aiken, G. R., Butler, K. D., Guillemette, F., Podgorski, D. C., & Spencer, R. G. M. (2016). DOM composition and transformation in boreal forest soils: The effects of temperature and organic-horizon decomposition state. *Journal of Geophysical Research: Biogeosciences*, *121*, 2727–2744. https://doi.org/10.1002/2016JG003431

Olefeldt, D., Goswami, S., Grosse, G., Hayes, D., Hugelius, G., Kuhry, P., et al. (2016). Circumpolar distribution and carbon storage of thermokarst landscapes. *Nature Communications*, *7*(1). https://doi.org/10.1038/ncomms13043

Quast, C., Pruesse, E., Yilmaz, P., Gerken, J., Schweer, T., Yarza, P., et al. (2012). The SILVA ribosomal RNA gene database project: Improved data processing and web-based tools. *Nucleic Acids Research*, *41*(D1), D590–D596. https://doi.org/10.1093/nar/gks1219

Rinke, C., Schwientek, P., Sczyrba, A., Ivanova, N. N., Anderson, I. J., Cheng, J. F., et al. (2013). Insights into the phylogeny and coding potential of microbial dark matter. *Nature*, *499*(7459), 431–437. https://doi.org/10.1038/nature12352

Rivkina, E., Gilichinsky, D., Wagener, S., Tiedje, J., & McGrath, J. (1998). Biogeochemical activity of anaerobic microorganisms from buried permafrost sediments. *Geomicrobiology Journal*, *15*(3), 187–193. https://doi.org/10.1080/01490459809378075

Rivkina, E. M., Friedmann, E. I., McKay, C. P., & Gilichinsky, D. A. (2000). Metabolic activity of permafrost bacteria below the freezing point. *Applied and Environmental Microbiology*, *66*(8), 3230–3233. https://doi.org/10.1128/AEM.66.8.3230-3233.2000

Rojas, P., Rodríguez, N., de la Fuente, V., Sánchez-Mata, D., Amils, R., & Sanz, J. L. (2018). Microbial diversity associated with the anaerobic sediments of a soda lake (Mono Lake, California, USA). *Canadian Journal of Microbiology*, *64*(6), 385–392. https://doi.org/10.1139/cjm-2017-0657

Salvadó, J. A., Tesi, T., Andersson, A., Ingri, J., Dudarev, O. V., Semiletov, I. P., & Gustafsson, Ö. (2015). Organic carbon remobilized from thawing permafrost is resequestered by reactive iron on the Eurasian Arctic Shelf. *Geophysical Research Letters*, *42*, 8122–8130. https://doi.org/10.1002/2015GL066058

Santi-Temkiv, T., Finster, K., Dittmar, T., Hansen, B. M., Thyrhaug, R., Nielsen, N. W., & Karlson, U. G. (2013). Hailstones: A window into the microbial and chemical inventory of a storm cloud. *PLOS One*, *8*(1). https://doi.org/10.1371/journal.pone.0053550

Schädel, C., Bader, M. K. F., Schuur, E. A. G., Biasi, C., Bracho, R., Čapek, P., et al. (2016). Potential carbon emissions dominated by carbon dioxide from thawed permafrost soils. *Nature Climate Change*, *6*(10), 950–953. https://doi.org/10.1038/nclimate3054

Schädel, C., Schuur, E. A. G., Bracho, R., Elberling, B., Knoblauch, C., Lee, H., et al. (2014). Circumpolar assessment of permafrost C quality and its vulnerability over time using long-term incubation data. *Global Change Biology*, *20*(2), 641–652. https://doi.org/10.1111/gcb.12417

Schaefer, K., Lantuit, H., Romanovsky, V. E., Schuur, E. A. G., & Witt, R. (2014). The impact of the permafrost carbon feedback on global climate. *Environmental Research Letters*, *9*(8), 085003. https://doi.org/10.1088/1748-9326/9/8/085003

Schirrmeister, L., Froese, D., Tumskoy, V., Grosse, G., & Wetterich, S. (2013). Yedoma: Late Pleistocene ice-rich syngenetic permafrost of Beringia. In S. Elias, C. Mock, & J. Murton (Eds.), *Encyclopedia of Quaternary Science* (2nd ed., 3888 p.). Amsterdam: Elsevier. https://doi.org/10.1016/B978-0-444-53643-3.00106-0

Schirrmeister, L., Kunitsky, V., Grosse, G., Wetterich, S., Meyer, H., Schwamborn, G., et al. (2011). Sedimentary characteristics and origin of the late Pleistocene Ice Complex on north-east Siberian Arctic coastal lowlands and islands—A review. *Quaternary International*, *241*(1-2), 3–25. https://doi.org/10.1016/j.quaint.2010.04.004

Schirrmeister, L., Meyer, H., Andreev, A., Wetterich, S., Kienast, F., Bobrov, A., et al. (2016). Late Quaternary paleoenvironmental records from the Chatanika River valley near Fairbanks (Alaska). *Quaternary Science Reviews*, *147*, 259–278. https://doi.org/10.1016/j.quascirev.2016.02.009

Schirrmeister, L., Schwamborn, G., Overduin, P. P., Strauss, J., Fuchs, M. C., Grigoriev, M., et al. (2017). Yedoma Ice Complex of the Buor Khaya Peninsula (southern Laptev Sea). *Biogeosciences*, *14*(5), 1261–1283. https://doi.org/10.5194/bg-14-1261-2017

Schneider von Deimling, T., Grosse, G., Strauss, J., Schirrmeister, L., Morgenstern, A., Schaphoff, S., et al. (2015). Observation-based modelling of permafrost carbon fluxes with accounting for deep carbon deposits and thermokarst activity. *Biogeosciences*, *12*(11), 3469–3488. https://doi.org/10.5194/bg-12-3469-2015

Schuur, E. A. G., McGuire, A. D., Schädel, C., Grosse, G., Harden, J. W., Hayes, D. J., et al. (2015). Climate change and the permafrost carbon feedback. *Nature*, *520*(7546), 171–179. https://doi.org/10.1038/nature14338

Spencer, R. G. M., Mann, P. J., Dittmar, T., Eglinton, T. I., McIntyre, C., Holmes, R. M., et al. (2015). Detecting the signature of permafrost thaw in Arctic rivers. *Geophysical Research Letters*, *42*, 2830–2835. https://doi.org/10.1002/2015GL063498

Stapel, J. G., Schirrmeister, L., Overduin, P. P., Wetterich, S., Strauss, J., Horsfield, B., & Mangelsdorf, K. (2016). Microbial lipid signatures and substrate potential of organic matter in permafrost deposits: Implications for future greenhouse gas production. *Journal of Geophysical Research: Biogeosciences*, *121*, 2652–2666. https://doi.org/10.1002/2016JG003483

Stapel, J. G., Schwamborn, G., Schirrmeister, L., Horsfield, B., & Mangelsdorf, K. (2017). Substrate potential of Eemian to Holocene permafrost organic matter for future microbial greenhouse gas production. *Biogeosciences Discussions*, 1–29. https://doi.org/10.5194/bg-2017-89

Steinberg, L. M. & Regan, J. M. (2008). Phylogenetic comparison of the methanogenic communities from an acidic, oligotrophic fen and an anaerobic digester treating municipal wastewater sludge. https://doi.org/10.1128/AEM.00553-08

Strauss, J., Schirrmeister, L., Grosse, G., Fortier, D., Hugelius, G., Knoblauch, C., et al. (2017). Deep Yedoma permafrost: A synthesis of depositional characteristics and carbon vulnerability. *Earth Science Reviews*, *172*, 75–86. https://doi.org/10.1016/j.earscirev.2017.07.007

Strauss, J., Schirrmeister, L., Mangelsdorf, K., Eichhorn, L., Wetterich, S., & Herzschuh, U. (2015). Organic-matter quality of deep permafrost carbon—A study from Arctic Siberia. *Biogeosciences*, *12*(7), 2227–2245. https://doi.org/10.5194/bg-12-2227-2015

Stubbins, A., Spencer, R. G. M., Chen, H., Hatcher, P. G., Mopper, K., Hernes, P. J., et al. (2010). Illuminated darkness: Molecular signatures of Congo River dissolved organic matter and its photochemical alteration by ultrahigh precision mass spectrometry. *Limnology and Oceanography*, *55*(4), 1467–1477. https://doi.org/10.4319/lo.2010.55.4.1467

Szymański, W. (2017). Quantity and chemistry of water-extractable organic matter in surface horizons of Arctic soils under different types of tundra vegetation—A case study from the Fuglebergsletta coastal plain (SW Spitsbergen). *Geoderma*, *305*, 30–39. https://doi.org/10.1016/j.geoderma.2017.05.038

Vermeire, M.-L., Bonneville, S., Stenuit, B., Delvaux, B., & Cornélis, J. T. (2019). Is microbial reduction of Fe (III) in podzolic soils influencing C release? *Geoderma*, *340*, 1–10. https://doi.org/10.1016/j.geoderma.2018.12.045

Vonk, J. E., Mann, P. J., Davydov, S., Davydova, A., Spencer, R. G. M., Schade, J., et al. (2013). High biolability of ancient permafrost carbon upon thaw. *Geophysical Research Letters*, *40*, 2689–2693. https://doi.org/10.1002/grl.50348

Vonk, J. E., Tesi, T., Bröder, L., Holmstrand, H., Hugelius, G., Andersson, A., et al. (2017). Distinguishing between old and modern permafrost sources in the northeast Siberian land–shelf system with compound-specific δ^2H analysis. *The Cryosphere*, *11*(4), 1879–1895. https://doi.org/10.5194/tc-11-1879-2017

Wagner, D., Gattinger, A., Embacher, A., Pfeiffer, E. M., Schloter, M., & Lipski, A. (2007). Methanogenic activity and biomass in Holocene permafrost deposits of the Lena Delta, Siberian Arctic and its implication for the global methane budget. *Global Change Biology*, *13*(5), 1089–1099. https://doi.org/10.1111/j.1365-2486.2007.01331.x

Waldrop, M. P., Wickland, K. P., White Iii, R., Berhe, A. A., Harden, J. W., & Romanovsky, V. E. (2010). Molecular investigations into a globally important carbon pool: permafrost-protected carbon in Alaskan soils. *Global Change Biology*, *16*, 2543–2554. https://doi.org/10.1111/j.1365-2486.2009.02141.x

Walter Anthony, K., Daanen, R., Anthony, P., Schneider von Deimling, T., Ping, C. L., Chanton, J. P., & Grosse, G. (2016). Methane emissions proportional to permafrost carbon thawed in Arctic lakes since the 1950s. *Nature Geoscience*, *9*(9), 679–682. https://doi.org/10.1038/ngeo2795

Walter Anthony, K., Schneider von Deimling, T., Nitze, I., Frolking, S., Emond, A., Daanen, R., et al. (2018). 21st-century modeled permafrost carbon emissions accelerated by abrupt thaw beneath lakes. *Nature Communications*, *9*(1), 3262. https://doi.org/10.1038/s41467-018-05738-9

Walter Anthony, K. M., Zimov, S. A., Grosse, G., Jones, M. C., Anthony, P. M., Chapin, F. S. III, et al. (2014). A shift of thermokarst lakes from carbon sources to sinks during the Holocene epoch. *Nature*, *511*(7510), 452–456. https://doi.org/10.1038/nature13560

Wang, J., Song, C., Hou, A., & Wang, L. (2014). CO_2 emissions from soils of different depths of a permafrost peatland, northeast China: Response to simulated freezing-thawing cycles. *Journal of Plant Nutrition and Soil Science*, *177*(4), 524–531. https://doi.org/10.1002/jpln.201300309

Wei, S., Cui, H., Zhu, Y., Lu, Z., Pang, S., Zhang, S., et al. (2018). Shifts of methanogenic communities in response to permafrost thaw results in rising methane emissions and soil property changes. *Extremophiles*, *22*(3), 447–459. https://doi.org/10.1007/s00792-018-1007-x

Willerslev, E., Hansen, A. J., Rønn, R., Brand, T. B., Barnes, I., Wiuf, C., et al. (2004). Long-term persistence of bacterial DNA. *Current Biology*, *14*(1), R9–R10. https://doi.org/10.1016/j.cub.2003.12.012

Xiang, X., Wang, R., Wang, H., Gong, L., Man, B., & Xu, Y. (2017). Distribution of *Bathyarchaeota* communities across different terrestrial settings and their potential ecological functions. *Scientific Reports*, *7*(1). https://doi.org/10.1038/srep45028

Zhang, J., Kobert, K., Flouri, T., & Stamatakis, A. (2014). PEAR: A fast and accurate Illumina Paired-End reAd mergeR. *Bioinformatics*, *30*(5), 614–620. https://doi.org/10.1093/bioinformatics/btt593

Zheng, J., Thornton, P. E., Painter, S. L., Gu, B., Wullschleger, S. D., & Graham, D. E. (2019). Modeling anaerobic soil organic carbon decomposition in Arctic polygon tundra: Insights into soil geochemical influences on carbon mineralization. *Biogeosciences*, *16*(3), 663–680. https://doi.org/10.5194/bg-16-663-2019

Zhou, J., Bruns, M. A., & Tiedje, J. M. (1996). DNA recovery from soils of diverse composition. *Applied and Environmental Microbiology*, *62*(2), 316–322.

Zimov, S. A., Davydov, S. P., Zimova, G. M., Davydova, A. I., Schuur, E. A. G., Dutta, K., & Chapin, F. S. III (2006). Permafrost carbon: Stock and decomposability of a globally significant carbon pool. *Geophysical Research Letters*, *33*, L20502. https://doi.org/10.1029/2006GL027484